Meteorologische Zeitschrift, Vol. **20**, No. 2, 227-241 (April 2011)

Article

Simulation of non-local effects of convection with the hybrid mass flux convection scheme HYMACS

VOLKER KUELL* and ANDREAS BOTT

Institute for Meteorology, University of Bonn, Germany

(Manuscript received June 29, 2010; in revised form October 5, 2010; accepted October 11, 2010)

Abstract

The hybrid mass flux convection scheme HYMACS has been proposed to simulate moist convection in non-hydrostatic numerical weather prediction models with grid sizes at which convection is partially resolved. Different to classical mass flux schemes HYMACS produces a net convective mass flux due to updrafts and downdrafts with resulting grid-scale pressure gradient forces. Thus, as a grid-scale reaction the environmental subsidence may cover several grid columns. Here, HYMACS is extended concerning the non-local effects of gust fronts and cell transport and aging in a way that convective cells can communicate also directly on the subgrid-scale without passing information only via grid-scale averages. Subgrid scale information of gust fronts from parameterized convective cells is used to initiate secondary cells by distributing a "trigger bonus" to neighboring grid columns. In addition, a cell age is assigned to convective cells to parameterize a temporal development in cloud top height and precipitation. This cell age is then transported on the grid-scale to simulate the advection of convective cells. The extentions of HYMACS are demonstrated by means of both idealized and real case experiments.

Zusammenfassung

Das hybride Massefluss-Konvektionsschema HYMACS wurde entwickelt, um Feuchte-Konvektion in nichthydrostatischen numerischen Wettervorhersagemodellen mit Gitterweiten zu simulierieren, bei denen Konvektion bereits teilweise aufgelöst wird. Im Unterschied zu klassischen Massefluss-Schemata produziert HYMACS einen konvektiven Netto-Massefluss aufgrund der konvektiven Auf- und Abwärtsströmungen, die dann gitterskalige Druckgradientenkräfte erzeugen. Daher kann die umgebende Subsidenz als gitterskalige Reaktion mehrere Gittersäulen bedecken. Hier wird HYMACS erweitert im Hinblick auf nichtlokale Effekte von Böenfronten und Zellentransport und -alterung insofern, dass konvektive Zellen auch direkt auf der Subgitterskala kommunizieren können, ohne Information ausschließlich über gitterskalige Mittelwerte austauschen zu müssen. Die subgitterskalige Information von Böenfronten parametrisierter konvektiver Zellen wird zur Initiierung sekundärer Zellen genutzt, indem ein "Trigger-Bonus" an die benachbarten Gittersäulen verteilt wird. Zusätzlich wird den konvektiven Zellen ein Zellenalter zugewiesen, um eine zeitliche Entwicklung der Wolkenoberkantenhöhe und des Niederschlags zu parametrisieren. Dieses Zellenalter wird dann auf der Gitterskala transportiert, um die Advektion der Zellen zu simulieren. Diese Erweiterungen von HYMACS werden anhand von idealisierten Experimenten und realen Fallstudien vorgeführt.

1 Introduction

The problem how to represent moist convection in numerical weather prediction (NWP) models has accompanied meteorological modelling during its whole history. On the one hand its effect is significant on both local scales as a source of severe weather up to large scales as a part of the global circulation (tropical convection) (e.g. CHARNEY and ELIASSEN, 1964; MANABE et al., 1965; KUO, 1965). This necessitates the inclusion of moist convection in limited area NWP models and global models. On the other hand, convective cells usually are of subgrid-scale, which necessitates their parameterization. Even with spatially limited models reaching grid sizes of a few 100 m in the future, which may simulate convection explicitly (BRYAN et al., 2003), the coarser resolved models used for nesting as well as global or climate models will always have to rely on parameterized convection (BECHTOLD et al., 2001).

Since the early days of NWP a number of convection parameterizations have been developed. These comprise both adjustment schemes (e.g. MANABE and STRICKLER, 1964; KUO, 1965; BETTS, 1986), which adjust convective profiles towards prescribed post-convective profiles taken from observations, and mass flux schemes (ARAKAWA and SCHUBERT, 1974; TIEDTKE, 1989; FRITSCH and CHAPPELL, 1980; GREGORY and ROWNTREE, 1990; BECHTOLD et al., 2001), which are driven by physical cloud models.

With grid resolutions of a few kilometers, as in contemporary NWP models, the problem of convection parameterization has become even harder, since convection now has become *partially resolved* on the grid. The continued use of classical parameterization schemes, which assume a zero net convective mass flux in the local grid column, leads to a conceptual problem (KAIN and FRITSCH, 1993). As the horizontal grid box area is

*Corresponding author: Volker Kuell, Institute for Meteorology, University of Bonn, Auf dem Hügel 20, 53121 Bonn, Germany, e-mail: vkuell@uni-bonn.de

0941-2948/2011/0212 $ 6.75

DOI 10.1127/0941-2948/2011/0212

no longer large enough to comprise especially the environmental subsidence of a convective cell, now a non-zero convective mass flux does exist in the local grid column due to updraft and downdraft.

To overcome this problem the hybrid mass flux convection scheme (HYMACS) has been developed (KUELL et al., 2007; KUELL and BOTT, 2008, 2009), which parameterizes only the updraft and downdraft with a net local mass flux and thus drives the environmental subsidence via pressure gradient forces on the grid-scale. The environmental subsidence closing the convective mass circulation now may cover several grid boxes and is no longer limited to the artificial scale of the model grid size. This leads to a more realistic dynamical behavior of the parameterization schemes and the hosting NWP model, which is also much less depending on the chosen grid size.

Another hybrid approach has been proposed by MONCRIEFF and LIU (2006) who apply a thermal forcing (baroclinic heating couplet) to improve the grid-scale circulation using a convective adjustment scheme.

Besides spatial limitations concerning the representation of moist convection most classical convection parameterizations are local in time. If a convective cell is triggered and then *evolves* at all, it is then only driven by the evolution of the large scale environment without any *life cycle* of its own. To include such a life cycle of convective cells into HYMACS, we here introduce a cell aging effect and as cells may move across the grid during their lifetime, they carry their cell age with them. In a gust front parameterization subgrid-scale information of gust fronts from parameterized convective cells is used to initiate secondary cells by distributing a "trigger bonus" to neighboring grid columns.

Section 2 briefly introduces the hosting NWP model used for our simulations, summarizes the basic ideas of the hybrid approach and the former "local" version of HYMACS and then introduces the non-local effects considered in the gust front parameterization and cell aging/transport scheme. In Section 3 we study the non-local extensions of HYMACS by means of idealized and real case experiments.

2 Model

For our model experiments we have chosen the COSMO (Consortium for Small Scale Modelling) model of the German Meteorological Service (DWD, Deutscher Wetterdienst) as the hosting grid-scale model for HYMACS. COSMO is a non-hydrostatic, nonlinear, fully compressible NWP model (DOMS and SCHAETTLER, 2002) which is used by DWD for the operational weather forecasts. In its operational mode COSMO uses the convection scheme by TIEDTKE (1989) and includes the convection scheme by KAIN and FRITSCH (1993) as an option. For our studies we have implemented HYMACS into the COSMO model (version 4.11). We use COSMO in the COSMO-EU mode with a horizontal grid size of 7 km, 40 layers and a dynamical timestep of 40 s. As in the operational setup the convection scheme is called every ten timesteps.

2.1 Hybrid approach

With finer grid size, the mass circulation of a convective cell consisting of updraft and downdraft and a larger scale compensating environmental subsidence, becomes partially resolved on the grid. Especially the environmental subsidence may cover several grid columns rather than only the local one. This leads to the idea to only parameterize the smaller scale updraft and downdraft in the local grid column producing a non-zero local convective mass flux. The divergences of this parameterized mass flux are passed to the model grid driving a grid-scale environmental subsidence by means of grid-scale pressure gradient forces. Starting from the conservation of mass in the local grid column we get the (extended) grid-scale continuity equation for the grid-scale mass flux $\rho\mathbf{v}$ and the parameterized convective mass flux $\mathbf{J}^m_{conv}$:

$$\frac{\partial \rho}{\partial t} + \nabla \cdot (\rho \mathbf{v}) + \nabla \cdot \mathbf{J}^m_{conv} = 0 \qquad (2.1)$$

Here, ρ and $\mathbf{v}$ denote the grid-scale total density and wind velocity. In a given grid box, the convective density tendency exchanging mass between the parameterization scheme and the hosting model is then

$$\left.\frac{\partial \rho}{\partial t}\right|_{conv} = -\nabla \cdot \mathbf{J}^m_{conv} = -\left(\frac{1}{A}\frac{\partial M^u}{\partial z} + \frac{1}{A}\frac{\partial M^d}{\partial z}\right) \qquad (2.2)$$

with the convective updraft and downdraft mass flux M^u and M^d and the grid box area A. M^u and M^d then are expressed by the entrainment and detrainment rates from the cloud model.

This hybrid approach produces a realistic mass circulation and is also consistent with the picture of a convective cell as a gravity wave generator (KUELL et al., 2007).

For the enthalpy and the moisture components equations analoguous to Eq. (2.2) can be derived. Especially the convective density and enthalpy tendencies may be expressed as tendencies of pressure and temperature.

2.2 Updraft

We give here only a short summary and define some special cloud levels to refer to in the following sections. Environmental air collected from the updraft source layer (USL) forms the updraft. At every vertical level a saturation adjustment is performed to choose dry or moist adiabatic ascend. The updraft air becomes saturated at the lifting condensation level (LCL) defining the cloud base. At the level of free convection (LFC), buoyancy

becomes positive and accelerates the updraft up to the equilibrium temperature level (ETL), where the virtual temperatures of the updraft and the environment become equal.

In the cloud model the fluxes of the convectively transported quantities Ψ are integrated upwards in the updraft (and downwards in the downdraft) from the flux equations:

$$\frac{\partial(M^{u,d}\Psi^{u,d})}{\partial z} = \epsilon^{u,d}\Psi - \delta^{u,d}\Psi^{u,d} + S_{\Psi}^{u,d} \qquad (2.3)$$

Quantities with indices u, d belong to the updraft and downdraft, quantities without indices are grid-scale averages. Ψ represents the moisture components for moisture fluxes, enthalpy for heat fluxes, horizontal wind for momentum fluxes or just $\Psi = 1$ for mass fluxes. The source term S_Ψ denotes phase changes between the moisture components or exchanges between updraft and downdraft.

Between the LCL and ETL the updraft entrainment and detrainment rates ϵ^u and δ^u are parameterized similar to TIEDTKE (1989) with a turbulent mixing coefficient of $\mu_0^u = 1{\cdot}10^{-4}\mathrm{m}^{-1}$:

$$\begin{aligned} \epsilon^u &= \mu_0^u M^u \Delta z + \nabla_h \cdot (\rho \mathbf{v})(\Delta x)^2 \Delta z \\ \delta^u &= \mu_0^u M^u \Delta z \end{aligned} \qquad (2.4)$$

The turbulent mixing terms will be extended in section 2.6.

Here, ∇_h denotes the horizontal nabla operator and $(\Delta x)^2$ is the grid box area. Above the ETL, the updraft entrainment rate is set equal to zero. The updraft kinetic energy is calculated from the integrated buoyancy of the updraft air and mixing of updraft and environmental vertical momentum. When the kinetic energy of the updraft air is exhausted, the cloud top level (CTL) is reached and the updraft air is detrained to the environment.

2.3 Downdraft and precipitation

In each model layer of depth Δz between the LCL and the CTL a fraction α_{pr} = 0.6 of the cloud liquid water and ice in the updraft (with specific contents q_l^u, q_i^u) is converted to precipitation particles (rain and snow with specific contents q_r^u, q_s^u) using the parameterization by OGURA and CHO (1973), which is also used in the convection scheme by BECHTOLD et al. (2001).

$$\begin{aligned} \Delta q_r^u &= \alpha_{pr}\, q_l^u (1 - \exp(-c_{pr}\Delta z / w^u)) \\ \Delta q_s^u &= \alpha_{pr}\, q_i^u (1 - \exp(-c_{pr}\Delta z / w^u)) \end{aligned} \qquad (2.5)$$

The condensate to precipitation conversion coefficient is set to c_{pr} = 0.04. w^u is the updraft vertical wind.

As in the scheme by BECHTOLD et al. (2001) precipitation is switched off for clouds with a depth of less than 3000 m which are considered as shallow convection. In each layer between the LCL and CTL the precipitation together with a fraction of the updraft air is split off to supply a downdraft mass flux. Down to the LCL, at each level an amount of environmental air equal to the air passed from the updraft is entrained and additional turbulent mixing similar to TIEDTKE (1989) is applied.

The downdraft is cooled by precipitation sublimating and evaporating according to a predefined relative humidity profile. Below the LCL all downdraft entrainment terms are set to zero.

The remaining precipitation is integrated from the CTL down to the surface and passed to the hosting model.

Concerning the kinetic energy, the downdraft is treated similarly to the updraft (integration of buoyancy and mixing of vertical momentum). When the kinetic energy is exhausted, the downdraft air is detrained back to the environment within the downdraft detrainment layer (DDL), the depth of which is set to 50 hPa as in BECHTOLD et al. (2001).

2.4 Trigger and closure

In HYMACS, the trigger function, which checks every grid box for instability able to initiate convection, consists of several contributions.

A test parcel with updraft air is lifted to the LCL, where a virtual temperature increment is added for buoyancy considerations only. If the parcel then reaches its LFC, convection is initiated. If not, the updraft is tried to be started from subsequent elevated levels to check for midlevel convection. The contributions to the virtual temperature increment account for:

i) large scale lifting (adopted from FRITSCH and CHAPPELL (1980) including the modification by KAIN (2004)).

ii) dynamic forcing by boundary layer turbulence. This is parameterized by an effective velocity $v_{TKE} = \sqrt{2\,\overline{TKE}}$ derived from the turbulent kinetic energy (TKE) averaged over the USL:

$$\Delta T_{v,TKE}^u = T^* \sqrt[3]{v_{TKE}} - T_0 \qquad (2.6)$$

To yield comparable temperature increment values as from the large scale lifting contribution we choose T^* = 5 K/$\sqrt[3]{100\ \mathrm{m\ s^{-1}}}$ and T_0 = 1 K and limit $\Delta T_{v,TKE}^u$ to 3 K at maximum.

A third contribution due to the effects of gust fronts from nearby cold pools will be added in section 2.5.

To fix the absolute values of the mass, heat and moisture fluxes we use a horizontal mass flux convergence closure for the updraft mass flux M_{LCL}^u at the LCL (from which all other fluxes are derived).

For more details of the hybrid approach and cloud model we refer to KUELL et al. (2007); KUELL and BOTT (2008).

2.5 Gust front parameterization

We now come to the modifications of HYMACS compared to the status described in KUELL and BOTT (2009). The trigger criterions mentioned above both rely on prognostic variables (w and TKE) in terms of local grid-scale averages. In contrast, a gust front may trigger convection in the *local* grid box, although the corresponding cold pool stems from a downdraft in a *neighbor* grid box. In addition, the sharp gradients at the gust front represent *subgrid-scale* information which will be lost after the *grid-scale* averaging, i.e. after adding any subgrid-scale tendencies from a parameterization to grid-scale prognostic variables. To exploit this information, it has to be passed among the grid boxes directly and not via grid-scale averages.

For every convective grid column with a parameterized downdraft our gust front parameterization derives a "trigger bonus" from the subgrid-scale downdraft quantities to be passed to the nearest neighbor grid columns. This is to lead the initiation of new cells and thus the propagation of cell clusters into directions which are favored by the outflow of nearby cold pools. This makes HYMACS a non-local scheme in which parameterized convection cells can communicate directly on the subgrid-scale.

Following WEISMAN and ROTUNNO (2004) the one-dimensional propagation velocity c of a cold pool boundary is derived from the conservation of energy:

$$\frac{1}{2}\,c^2 = \int_0^h -B\,dz = g\int_0^h \frac{T_v - T_v^d}{T_v}\,dz \qquad (2.7)$$

Here, B denotes the buoyancy and T_v^d and T_v are the virtual temperatures of the downdraft and of the environment. The depth h of the cold pool is assumed to be equal to the depth of the DDL. Collecting possible cold pool mass fluxes and kinetic energy from all eight neighbors (at the edges and corners) results in a cold pool velocity contribution $\mathbf{c}_i$ from the ith neighbor grid column:

$$\mathbf{c}_i = \mathbf{e}_i \sqrt{\frac{1}{4}\,\alpha\,\Delta z_{DDL}\,g\,\frac{\overline{T_v} - \overline{T_{v,i}^d}}{\overline{T_v}}} \qquad (2.8)$$

The unit vectors $\mathbf{e}_i$ point from the eight surrounding neighbor grid boxes to the local target grid box, the total trigger bonus of which is to be determined. $\overline{T_v}$ and $\overline{T_{v,i}^d}$ are the virtual temperatures of the local grid box and of the downdraft in the ith neighbor grid box (both averaged over the depth of the DDL). To obtain cold pool velocities comparable to the background wind shear at the cold front, we have introduced a scaling factor α = 2 which has been adjusted for the strong cold front of the case study of July 20, 2007 discussed below in Section 3.2.1. The total cold pool velocity at the local grid box then is

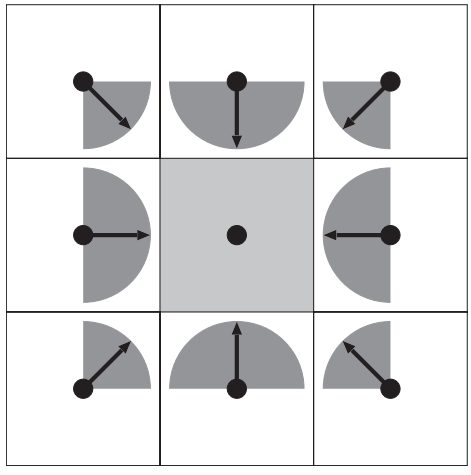

Figure 1: Definition of upstream grid boxes relative to the local (light grey) grid box. If the propagation velocity vector $\mathbf{v}_{p,i}$ in a neighbor grid box points into a direction within the grey marked ranges, the grid box is considered to be located upstream. Black arrows denote the vectors $\mathbf{e}_i$. For details see text.

$$\mathbf{c} = \sum_{i=1}^{8} \mathbf{c}_i \qquad (2.9)$$

To initiate a secondary convective cell, the cold pool velocity $\mathbf{c}$ has to be parallel and of similar absolute value to the mean low level background wind shear (WEISMAN and ROTUNNO, 2004). With $\Delta\mathbf{v_h}$ being the shear of the horizontal wind (integrated over the DDL) an effectivity η is parameterized by a bell shaped distribution around the "optimal" value $\mathbf{c} = \Delta\mathbf{v_h}$.

$$\eta = \frac{1}{1 + \frac{(\mathbf{c}-\Delta\mathbf{v_h})^2}{\Delta_0^2}} \qquad (2.10)$$

The half width of the bell curve has been set to Δ_0 = 10ms^{-1}. Analoguously to the classical Fritsch-Chappell trigger contribution we choose for the trigger bonus due to gust fronts:

$$\Delta T_{v,GF}^u = \eta \sqrt[3]{\gamma_{GF}\,|\mathbf{c}|} \qquad (2.11)$$

To get absolute values in the range of the other trigger contributions, the scaling factor has been set to γ_{GF} = 200 sm^{-1}K^3. Since the trigger bonus is collected only from the nearest eight neighbors, the maximal cold pool velocity, that can be represented, is limited by the grid box size divided by the convective time step as a Courant-Friedrichs-Lewy criterion.

2.6 Cell aging and transport

A further non-local effect to be considered is the temporal development of convective cells and their advection

across the model grid. With the classical approach a recently triggered convective cell immediately has its final cloud top height and precipitation without any growth or evolution. If any temporal evolution is present at all, it is due to the evolution of the environmental conditions with which the cell is always in equilibrium. To smooth this extremely nonlinear cell behavior (non triggered/fully developed) we introduce a cell aging mechanism by means of an additional *time dependent* turbulent mixing term $\mu^*(t)$ in Eq. (2.4):

$$\begin{aligned} \epsilon^u &= (\mu^*(t) + \mu_0^u) M^u \Delta z + \nabla_h \cdot (\rho \mathbf{v}) (\Delta x)^2 \Delta z \\ \delta^u &= (\mu^*(t) + \mu_0^u) M^u \Delta z \end{aligned} \tag{2.12}$$

with

$$\mu^*(t) = \begin{cases} 2\mu_0^u (1 - \frac{t_{cell}}{\tau}) & : \quad t_{cell} < \tau \\ 0 & : \quad t_{cell} \geq \tau \end{cases} \tag{2.13}$$

This decreasing mixing follows the idea of a successive replacement of environmental air by cloud air in a developing convective cell. In addition, we damp the generation of precipitation for young clouds by scaling the condensate to precipitation conversion coefficient c_{pr} in Eq. (2.5) with a time dependent factor γ_{pr}.

$$\gamma_{pr}(t) = \begin{cases} 0.01 + 0.99 (\frac{t_{cell}}{\tau})^2 & : \quad t_{cell} < \tau \\ 1 & : \quad t_{cell} \geq \tau \end{cases} \tag{2.14}$$

For both time-dependent quantities $\mu^*(t)$ and $\gamma_{pr}(t)$ a typical value of τ = 20 min is chosen as the evolution time scale for a convective cloud.

To complete the whole picture of evolving and moving cells, an important part still is missing. A moving cell, i.e. a cell which is triggered in subsequent grid boxes, would now evolve again and again in each grid box. To make this cell grow only once and then move remaining in its mature state, its age has to be transported downstream with the cell. Convective cells usually move with the background wind at the height of their steering level, which here in a first approach is assumed to be located at a typical cloud center altitude of 500 hPa. Errors in the movement direction due to this approximation are neglected, since only the eight nearest neighbors of the local grid box are considered.

Let $\mathbf{v}_{p,i}$ be the normalized propagation velocity vector of the convective cell in the ith neighbor grid box and the unit vectors $\mathbf{e}_i$ point from the ith neighbor grid box to the local grid box. The scalar product $s_i = \mathbf{v}_{p,i} \cdot \mathbf{e}_i$ can now be used to define a weighting factor α_i for the ith neighbor grid box deciding if (and to which extent) it is to be considered as an upstream grid box, i.e. existing convective cells in this neighbor grid box may exert an influence on the age of a cell triggered in the local grid box (see Fig. 1). For direct neighbor grid boxes $\mathbf{v}_{p,i}$ has to deviate less than ϕ = 90° from $\mathbf{e}_i$ (i.e. $s_i = \cos(\phi) > 0$), whereas for diagonal neighbor grid boxes $\mathbf{v}_{p,i}$ has to deviate less than only ϕ = 5° from $\mathbf{e}_i$ (i.e. $2s_i^2 - 1 = \cos(2\phi) > 0$).

Table 1: Propagation of cell age

local cell present	upstream convective activity	new local cell age
no	no	0
yes	no	$t_{old} + \Delta t$
no	yes	$\max_{i=1,8}(s_i t_i)$
yes	yes	$\max_{i=1,8}(t_{old} + \Delta t, s_i t_i)$

Δt is the time step (since the last call of the convection scheme).

$$\alpha_i = \begin{cases} s_i & : s_i > 0 \quad \text{and } i \text{ is direct neighbor} \\ 2s_i^2 - 1 & : 2s_i^2 - 1 > 0 \\ & \text{and } i \text{ is diagonal neighbor} \\ 0 & : \quad \text{else} \end{cases} \tag{2.15}$$

Since cell age certainly is not an additive quantity, if two cells interact, we here choose the simple approach that the oldest (most mature) cell is dominant. Thus, for several upstream cells with ages t_i interacting with the local cell with age t_{old}, the maximum age is assigned as the new local cell age (see Table 1).

Similar to the gust front parameterization also for the cell aging/transport scheme, for simplicity only the nearest eight neighbor grid boxes are considered here, thus limiting the maximum propagation velocity, that can be represented, to the grid box size divided by the convective time step. However, both the gust front parameterization and the cell aging/transport scheme are to favor or suppress the convective development into a certain direction *in addition* to the direction which is given by the grid-scale fields and the classical trigger criteria and the classical cloud model.

2.7 Momentum transport and radiative effects

Compared to the version of HYMACS presented in KUELL and BOTT (2009) we have completed the scheme by including convective momentum transport and radiative effects. Momentum is transported by convective updrafts and downdrafts as any other quantity like moisture or enthalpy. In addition, for momentum a subgrid-scale source has to be considered, as pressure gradient forces across the updraft and downdraft may represent a significant momentum source. This effect is parameterized with a source term in the convective momentum flux equations (cf. Eq. (2.3)) following GREGORY et al. (1997):

$$\left. \frac{\partial M^{u,d} \mathbf{v}_h^{u,d}}{\partial z} \right|_{source} = c_{mom} M^u \frac{\partial \mathbf{v}_h}{\partial z} \tag{2.16}$$

Here, $\mathbf{v}_h^{u,d}$ and $\mathbf{v}_h$ denote the horizontal wind in the updraft and downdraft and on the grid-scale. As in GREGORY et al. (1997) we choose c_{mom} = 0.7.

Radiative effects from convective clouds are considered by passing a convective cloud coverage to the radiation scheme in every model layer. The convective cloud coverage C_{conv} is derived geometrically by adding the updraft and downdraft area representing the horizontal cloud area.

$$C_{conv} = \frac{A^u + A^d}{(\Delta x)^2} \quad \text{with} \quad A^{u,d} = \frac{M^{u,d}}{\rho^{u,d} w^{u,d}} \tag{2.17}$$

The updraft and downdraft area A^u and A^d and the corresponding densities $\rho^{u,d}$ and vertical winds $w^{u,d}$ can all be directly determined from the cloud model. The primary quantities of the updraft and downdraft are the mass fluxes (from the closure assumption) and the densities (from the thermodynamics and virtual temperatures). From the densities of the drafts and the environment the buoyancies of the drafts and the vertical velocities are determined.

Since the downdraft is formed by precipitation (and/or cloud) particles evaporating into unsaturated air (producing cooling and negative buoyancy), the presence of liquid water (or ice) is a necessary prerequisite for the downdraft. Thus, we count the downdraft area as cloud area.

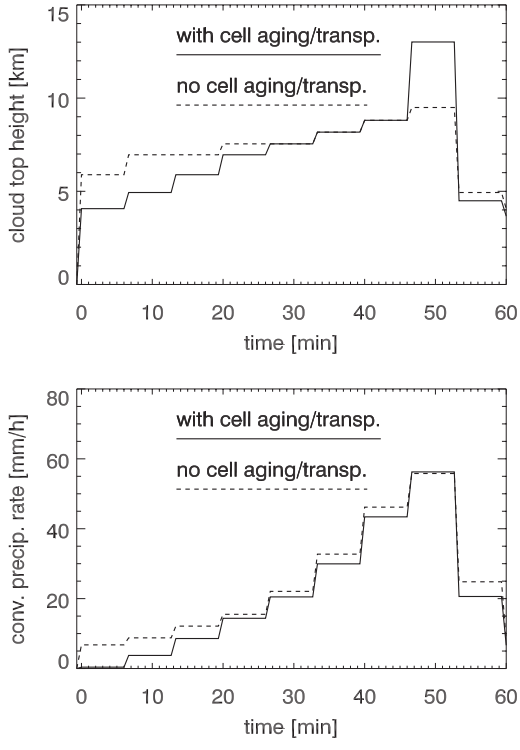

Figure 2: Intercomparison between a simulation with (solid lines) and without (dashed lines) cell aging. Evolution of the cloud top height (top) and convective precipitation (bottom) of the primary (center) convective cell with time relative to the initiation (triggering) of the cell.

3 Results

3.1 Idealized experiments

For our idealized experiments we choose a conditionally instable atmosphere as in WEISMAN and KLEMP (1982) with the specific water vapor content limited to 12 g kg^{-1} fixing the convective available potential energy (CAPE) at a medium value of about 1400 m^2 s^{-2}.

3.1.1 Cell aging and transport

In the first idealized experiment the background wind is set to zero and flat orography is assumed. To trigger convection in this horizontally homogeneous atmosphere, the temperature T in the boundary layer is superimposed with a positive disturbance ΔT with a radius r = 2 km and a maximum amplitude ΔT_0 = 2 K located at the domain center (x_0, y_0) and at a height $z_0 = r$:

$$\Delta T = \begin{cases} \Delta T_0 \cos(\frac{\pi}{2}\delta) & : \quad \delta < 1 \\ 0 & : \quad \text{else} \end{cases} \tag{3.1}$$

with

$$\delta = \frac{1}{r}\sqrt{(x-x_0)^2 + (y-y_0)^2 + (z-z_0)^2}$$

This warm air bubble triggers a convective cell at the center of the model domain (which afterwards triggers circular patterns of secondary cells, since the whole domain has been homogeneously initialized with a conditionally unstable atmosphere). The warm air bubble is constructed in a way that grid-scale precipitation does not start before one hour after the initialization of the convective cell. Thus, during the first hour there is no interference between the convective and grid-scale preciptation. During the first hour the center convective cell also is not affected by the secondary cells in terms of cell age, i.e. its cell age linearly increases with model time without any inheritance from neighbor cells (cf. Tab. 1).

Fig. 2 compares the temporal evolution of the cloud top height and convective precipitation for a simulation with and without cell aging. The gust front parameterization (cf. Section 3.1.2) is switched off here. A simulation with gust front parameterization shows no significant differences for the primary cell. Without cell aging both cloud top height and precipitation are only given by the evolution of the grid-scale conditions. The warm air bubble rises and causes a weak grid-scale vertical wind triggering the convection scheme. The grid-scale convergence below the bubble fixes the initial updraft source mass flux of the convective cell by means of the closure assumtion of HYMACS. This mass flux stays constant with $M^u_{LCL} = 9.2 \cdot 10^6$ kg s^{-1} for the first 46 min and then falls to $7.6{\cdot}10^6$ kg s^{-1} (not shown). After being triggered the convective cloud immediately starts with a cloud top height of 6000 m and then slowly increases to 9500 m. Precipitation starts with a rate of 7 mm h^{-1} and increases to a maximum of 56 mm h^{-1}.

However, with cell aging the cloud starts with a CTL height of z_{CTL} = 4000 m. With the LCL height of z_{LCL} = 800 m this results in a cloud depth of $z_{CTL} - z_{LCL}$ = 3200 m only slightly above the non-precipitating shallow convection limit of 3000 m (cf. Section 2.3). Although at the shallow convection limit of 3000 m precipitation would be forced to zero, at $z_{CTL} - z_{LCL}$ = 3200 m its intensity now falls to low values (0.5 mm h^{-1}) due to the cell aging parameterization without any additional forcing. This type of cloud evolution with a smooth transition from non-precipitating shallow convection to precipitating deep convection has been an important issue of moist convection modelling pointed out in literature (KUANG and BRETHERTON, 2006). As claimed by these authors we use the same convection scheme with the same parameter settings for both shallow and deep convection with the only assumption that in shallow convective clouds no cloud particles are converted to precipitation.

Generally, the cell aging parameterization delays the growth of cloud and the occurence of the maximum cloud top height and precipitation to later times than given by the grid-scale environment.

3.1.2 Gust front parameterization

To check the effect of our gust front parameterization, we set up an idealized experiment as in Section 3.1.1 with the difference that the background wind profile now is set to u = 20 m s^{-1} at all altitudes and the orography consists of a meridionally oriented ridge with a bell shaped profile of the surface height h centered at the middle of the model domain at $x = x_{max}/2$:

$$h(x) = h_{max} \frac{1}{1 + \frac{4}{b^2}(x - \frac{x_{max}}{2})^2} \qquad (3.2)$$

We choose a half width of the ridge of b = 56 km and its maximum height h_{max} = 1000 m. This results in a Froude number of Fr = 2.2. After CHEN and LIN (2005) this high Froude number together with medium CAPE results in precipitation areas located near the mountain peak and propagating downstream from the mountain (denoted as domain IV in their Figs 12 and 16). To also consider possible cold pool velocities equal to or exceeding u = 20 m s^{-1}, we here call HYMACS every 200 s instead of the operationally used intervall of 400 s for calling the convection scheme.

Fig. 3 compares our results with gust front parameterization and without (reference). Both with and without gust front parameterization the first convective cell at the top of the ridge is equally initiated after 33 min as an orographic effect in grid column 0 (see arrow in Fig. 3). In the case with gust front parameterization this cell triggers a secondary cell in the adjacent grid column 1. This cell then intensifies and dominates the cell in grid column 0. This cluster occupying one to two grid columns then moves further downstream. After 46 min it has reached grid column 2 and has again reduced to one grid column. This triggering of secondary cells is due to the cold pool of the respective upstream cell and is not observed without gust front parameterization. Without gust front parameterization the cell over the top of the ridge does also produce a cold pool but due to its subgrid-scale nature the only way to interact with neighbor grid columns is via grid-scale averages, which smooth out all information of sharp gradients as, e.g., gust fronts. Thus, without gust front parameterization no secondary cell is initiated. This would only have been the case, if the cold pool would have attained grid-scale size, which (depending on the chosen grid size) lasts much longer and need not occur anyway. Indeed, after more than one hour (after model initialization) also without gust front parameterization precipitation begins to spread downstream from the top of the ridge (not shown).

3.2 Real cases

3.2.1 Frontal convection

For our real case study of frontal convection we choose July 20, 2007 on which a strong cold front passes over Germany from the West to the East. This cold front is generated by a low associated with a mesoscale convective system located over north-eastern France. The cold front, which also develops a preceeding convergence line, causes strong deep convection with heavy precipitation. We here concentrate on orographically induced cells as they are initiated, e.g., over the Black Forest and then move north-eastwards.

Fig. 4 shows hourly precipitation sums from the model results of COSMO with HYMACS (with and without gust front parameterization and cell aging/transport) at 14:00 UTC and observations from the DWD precipitation network at 13:00 and 14:00 UTC. On this day, for COSMO the whole simulated front is generally about one hour behind the observed one. This is independent of the convection scheme used (also tested with the schemes by TIEDTKE (1989) (which also is used operationally) and KAIN and FRITSCH (1993), not shown). The cause of this is suspected in the driving data which is used for initialization and provision of the lateral boundary data (operational COSMO-EU analyses). As this is beyond the scope of the present paper, we here focus on the relative development of the convection cells rather than their exact temporal assignment to observed cells.

After the first simulated convective cells have been initiated over the Black Forest at about 11:00–12:00 UTC, they remain weak for several hours in the reference simulation, whereas in the simulation with gust front parameterization and cell aging/transport they grow rapidly and move downstream north-eastwards.

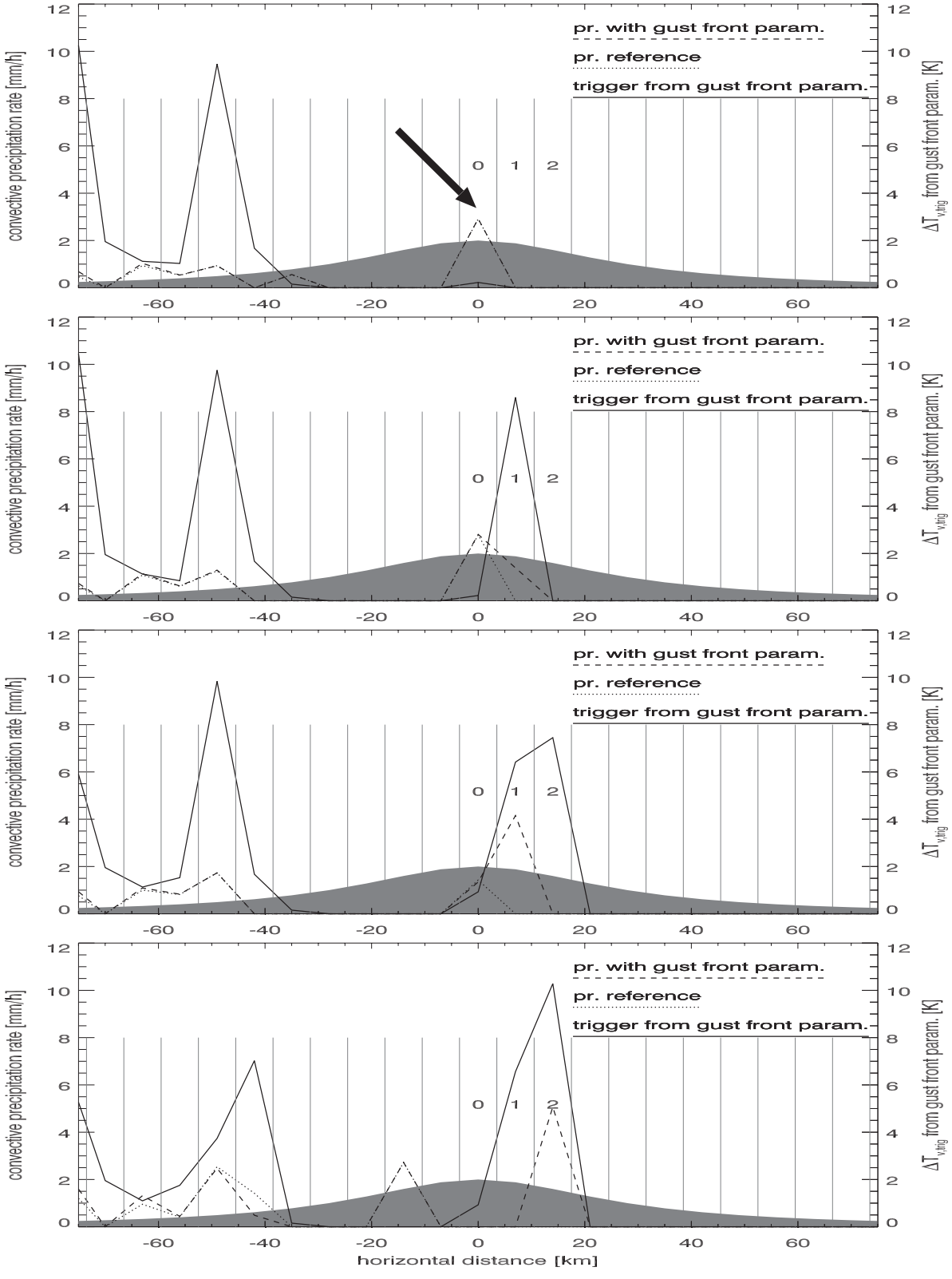

Figure 3: Intercomparison of convective precipitation (left y axis) between a simulation with (dashed lines) and without (dotted lines) gust front parameterization. The solid lines denote the trigger contribution from the gust front parameterization (right y axis). Shown are model states after 33, 36, 39, and 46 min after initialization (from top to bottom). The relative height of the ridge is shaded in grey. Grid column boundaries are plotted as vertical grey lines. The arrow shows the first convective cell at the top of the ridge in grid column 0 (see text).

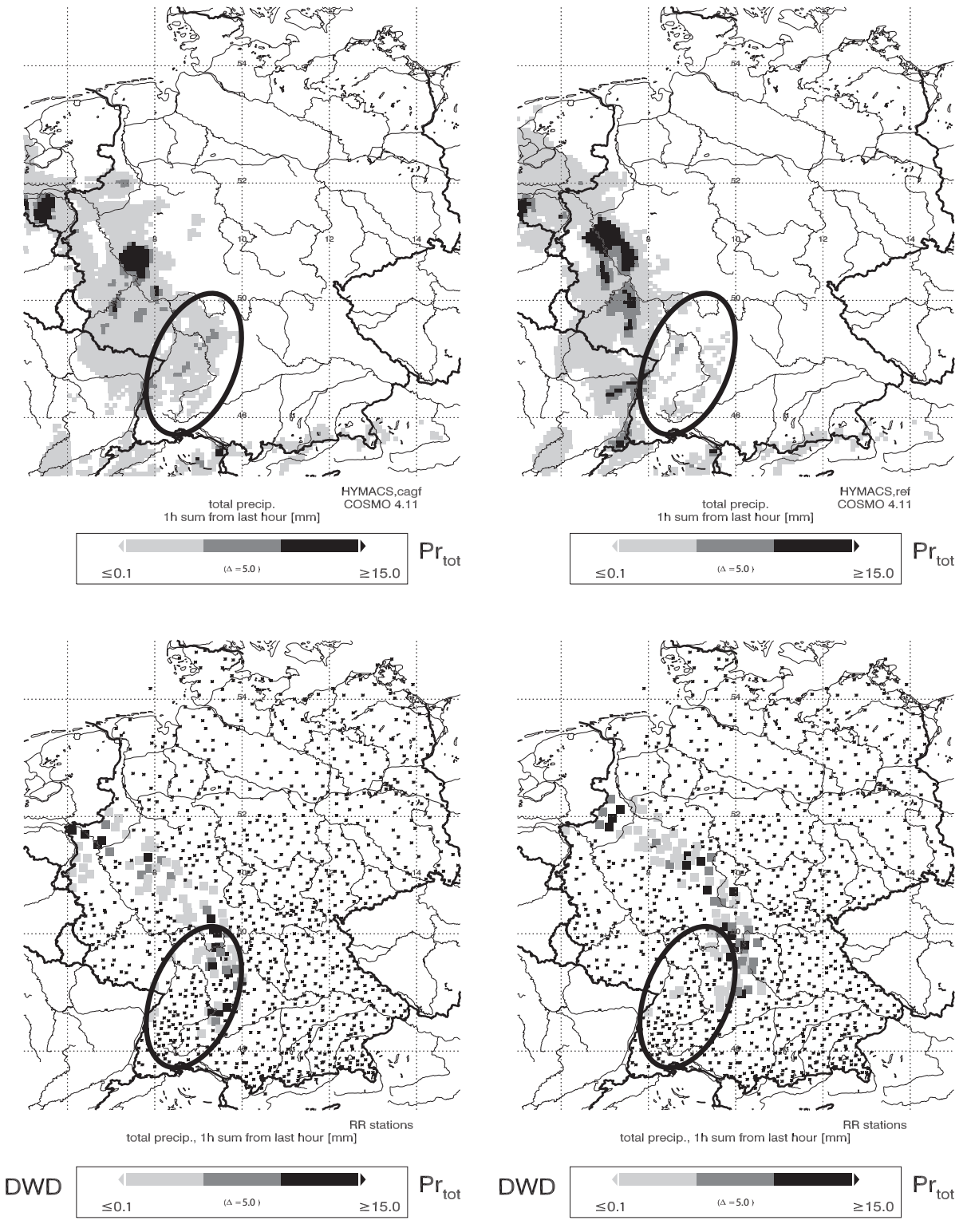

Figure 4: Intercomparison of total precipitation (1 h sums). The top panel shows COSMO simulation with HYMACS with (left) and without gust front parameterization and cell aging/transport (right) at 14:00 UTC on July 20, 2007. The bottom panel shows observed precipitation (1 h sums) from the DWD precipitation network at 13:00 (left) and 14:00 UTC (right). Asterisks denote location of station with precipitation below 0.1 mm h^{-1}.

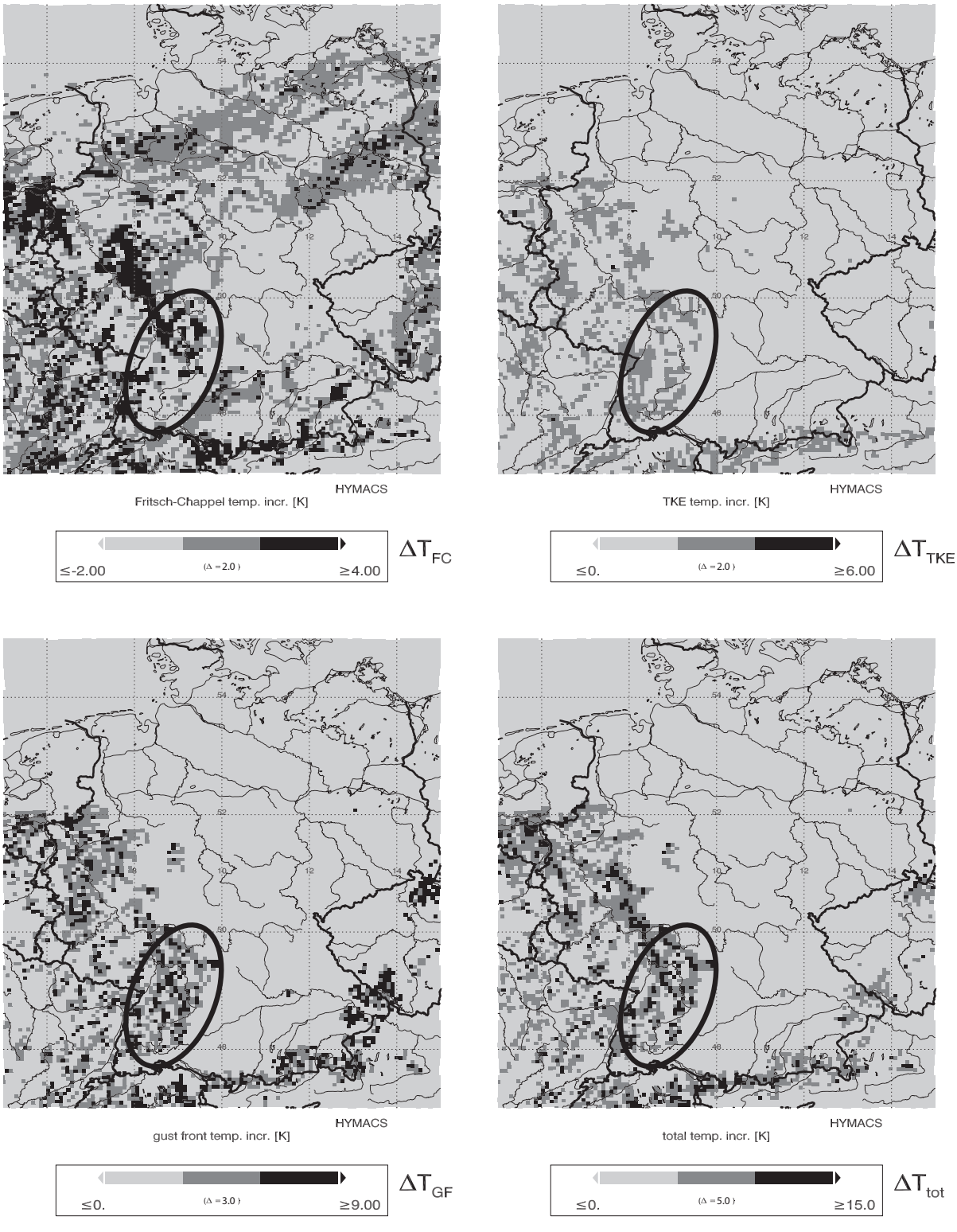

Figure 5: Virtual temperature increments at 14:00 UTC on July 20, 2007 from Fritsch-Chappel trigger (upper left), TKE trigger (upper right), gust front parameterization (lower left) and total (lower right). For details see text.

Focussing on the cells initiated downstream of the bow shaped front (i.e. encircled area in Fig. 4), Fig. 5 reveals the contributions from the different terms in the trigger function. In the northern part and at the ascending slope of the Black Forest a significant contribution comes from the Fritsch-Chappel trigger which is parameterized by the grid-scale vertical wind and thus also reacts on orographic lifting. In the eastern part of the encircled area (downstream of the ridge) the contribution from the Fritsch-Chappel trigger is small or even negative, i.e. inhibiting convection. The contribution from the TKE trigger term here is too small to initiate significant convection, as can be seen from the reference simulation (Figure 4, upper right map) which also does include the TKE term. The only stronger and area filling contribution, especially in the eastern part of the encircled area (downstream of the ridge), comes from the gust front parameterization. As in the idealized experiment cells once initiated near the ridge are enabled to initiate secondary cells downstream of the ridge.

Fig. 6 shows the distribution of cell age at the same time as in the analysis above. In the northern part of the front (north of 50°N), where the front and the convective cells move only slowly eastward, cell age increases gradually from east to west. In the southern part of the front (encircled area), where the cells are moving faster, cell age jumps to high values within only two grid points (14 km). This means that here most part of the cell age is "advected" from upstream grid points rather than accumulated at the local grid point. This also demonstrates the interaction between the gust front parameterization and the cell aging/transport algorithm. In case of strong background wind, cells which are triggered by the gust front parameterization mostly inherit the higher age of their generating (upstream) cells and, thus, they begin to precipitate earlier than cells in an environment with weak winds, whose age simply increases with proceeding model time at the local grid point. This accelerates the propagation of the leading edge of precipitation from cells driven by gust fronts to more realistic values compared to observations.

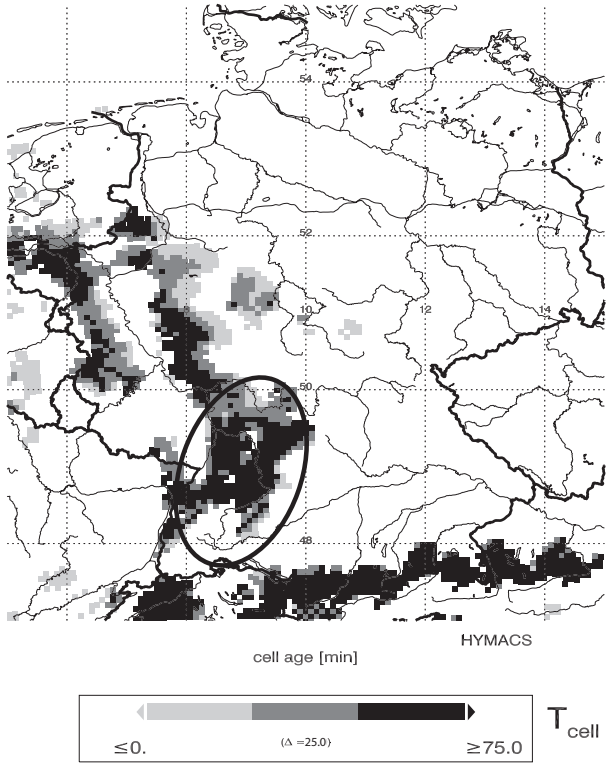

Figure 6: Cell age at 14:00 UTC on July 20, 2007. For details see text.

3.2.2 Airmass convection

For another real case study with airmass convection we choose the time period of Aug. 12/13, 2007. On Aug. 12 the synoptic situation is characterized by a high with its core moving from north-eastern France to north-western Germany with very moist subtropical air. Lifting is promoted by an upper low with its core over Serbia and an upper trough pointing towards eastern Germany. Fig. 7 shows the situation at 17:00 UTC as measured by the DWD precipitation network and simulated by COSMO with HYMACS (with and without gust front parameterization and cell aging/transport).

Focussing on the cells over the ridge of the Black Forest again (encircled in Fig. 7), the simulation with gust front parameterization and cell aging/transport again exhibits stronger precipitation compared to the reference run, although less pronounced than in the frontal case.

As can be seen from Fig. 8 the trigger contribution from the gust front parameterization here again plays the decisive role. The contribution from the Fritsch-Chappel trigger is only small or even negative. The TKE trigger contributes a few Kelvin, which does not suffice to start significant convection as the reference simulation (Figure 7, upper right map) reveals. It is the contribution from the gust front parameterization, which initiates stronger convection at and especially downstream of the Black Forest ridge (see encircled areas in Fig. 7, upper left map and Fig. 7).

4 Conclusions

The hybrid mass flux convection scheme (HYMACS) has been developed to overcome some conceptual problems of the classical convection schemes when used with grid sizes at which convection becomes partially resolvable. Different to the classical schemes it only parameterizes updrafts and downdrafts which result in a net convective mass flux driving the (larger scale) environmental subsidence on the grid-scale due to pressure gradient forces.

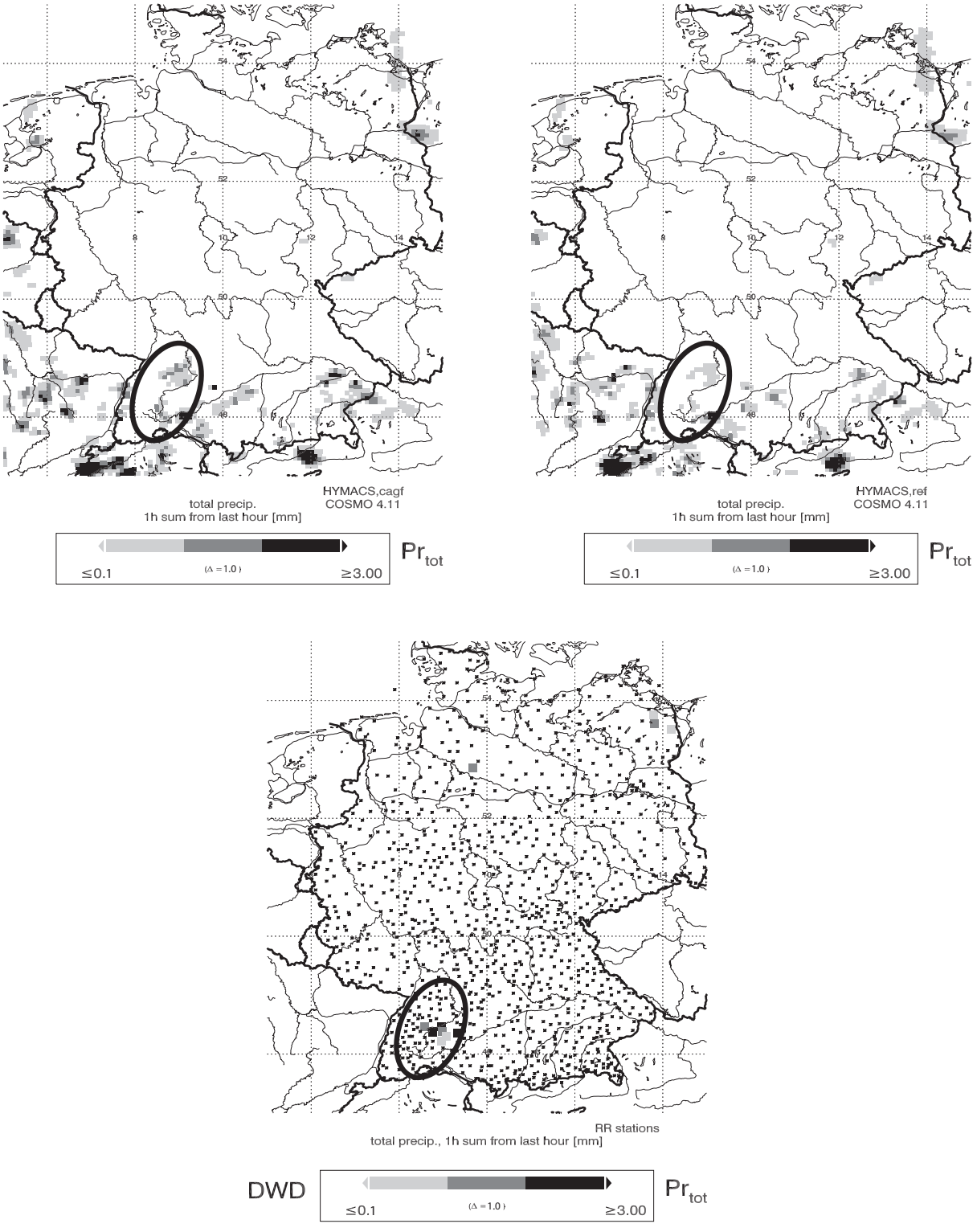

Figure 7: Intercomparison of total precipitation (1 h sums) at 17:00 UTC on Aug. 12, 2007. The top panel shows COSMO simulation with HYMACS with (left) and without gust front parameterization and cell aging/transport (right). The bottom panel shows observed precipitation (1 h sums) from the DWD precipitation network. Asterisks denote location of station with precipitation below 0.1 mm h^{-1}. For details see text.

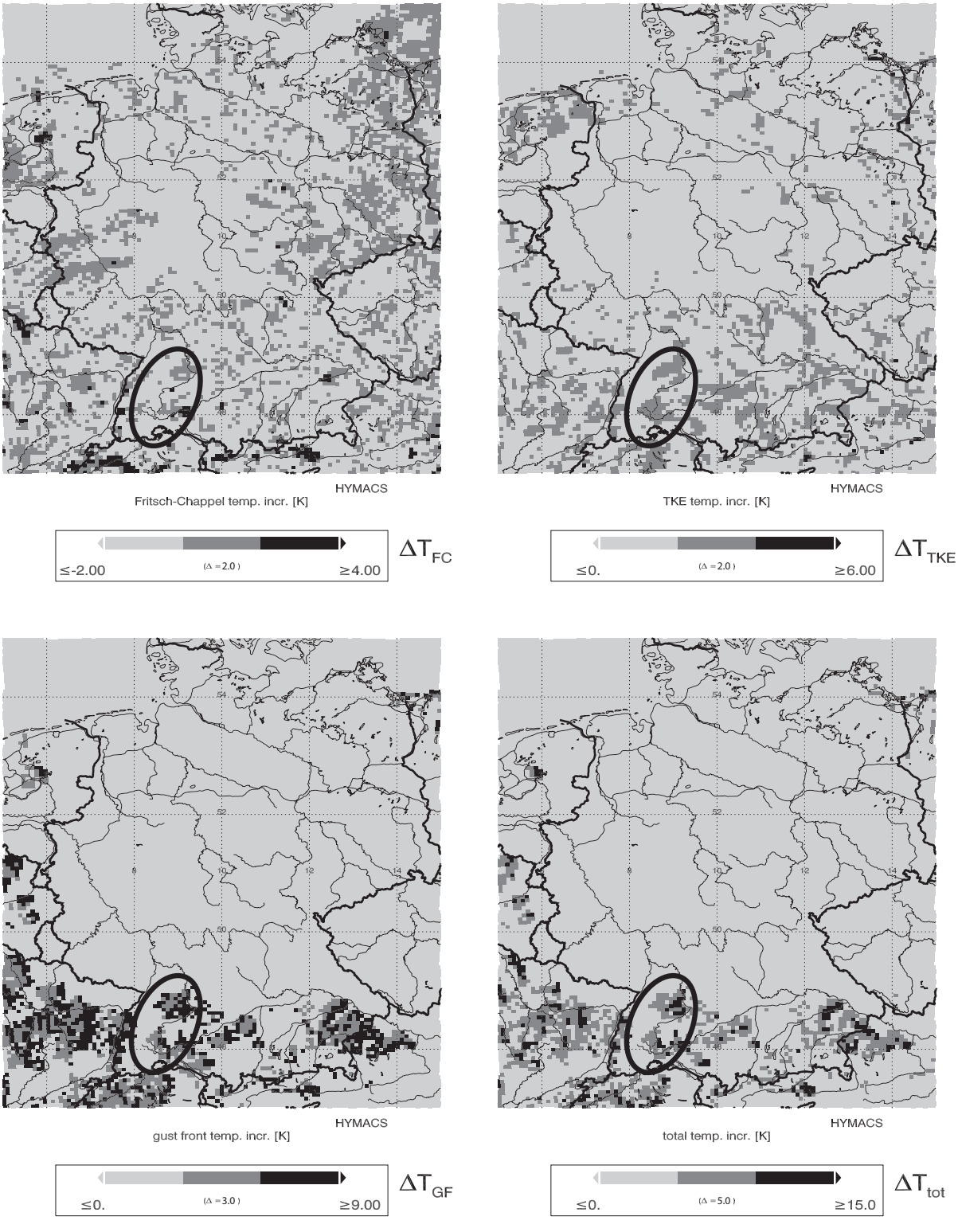

Figure 8: Virtual temperature increments at 17:00 UTC on Aug. 12, 2007 from Fritsch-Chappel trigger (upper left), TKE trigger (upper right), gust front parameterization (lower left) and total (lower right).For details see text.

Here, HYMACS is extended to a non-local scheme in both space and time, i.e. the scheme also interacts with neighbor grid columns rather than only the local one and considers the history of a cell and neigboring preexisting cells in terms of a transportable cell age.

The motivation for this is as follows: First, convective cells have an intrinsic life cycle, which allows the onset of precipitation after a certain "build-up" time of typically 20 min. In classical convection schemes the temporal development of a cell is solely determined by the behavior of the grid-scale environment. Especially, a cell may precipitate at full strength immediately after being triggered. To avoid this unrealistic behavior, we assign a cell age to every parameterized cell controlling the lateral mixing of the cloud with its environment and the generation of precipitation. As shown in an idealized experiment, this produces a gradual increase of the cloud top height and the precipitation rate. As this cell age is transported, when the cell moves across the grid, preexisting mature cells keep on precipitating when entering a new grid column.

Second, precipitating convective cells producing a spreading cold pool with a gust front can trigger secondary cells resulting in a long-living system. As cold pools or at least their sharp temperature gradient at the gust front usually are of subgrid-scale, this information will be lost when convective temperature tendencies are just added to the total temperature tendency, i.e. the cold pool temperature is averaged on the grid-scale. Thus, before averaging we use this subgrid-scale information for a gust front parameterization distributing a trigger bonus to the neigboring grid cells guiding convection in directions where the thermal stratification and the wind shear are favorable (cf. WEISMAN and ROTUNNO, 2004). Convection in an idealized flow over a mountain ridge demonstrates the downstream movement of such a cell cluster triggered at the ridge.

In two real case studies the effect and the interaction of the gust front parameterization and the cell aging/transport algorithm are demonstrated for orographically induced cells for both frontal and airmass convection. Compared to the former version of HYMACS, convection and precipitation are stronger at and downstream of the ridge (lee side). Cells initiated at the ridge trigger secondary cells by their cold pools which in turn trigger further cells and so on, resulting in a travelling system. Especially at locations with high propagation velocities cell age is mainly inherited from upstream cells rather than accumulated locally. Thus, the travelling cells or clusters quickly start to precipitate when reaching a new location different to isolated or slow moving cells (with less or no inheritance from upstream cells) which have to wait until their mature state is reached.

Compared to measurements of hourly precipitation sums the gust front parameterization and the cell aging/transport algorithm lead to a more realistic distribution and propagation of precipitation patterns confirming their behavior tested in the idealized experiments.

A limitation of HYMACS in its current version is reached for situations when the updraft or downdraft are no longer in the same grid box. The treatment of such cases represents a possible extension of HYMACS in the future for a smooth transition to explicitly resolved convection.

Acknowledgments

We thank the Deutscher Wetterdienst (DWD) for providing the COSMO model system and driving data and station data of precipitation (SYNOP data). We gratefully acknowledge the very constructive referee comments. Our work was funded by grant Bo998/7-1, Bo998/7-2 and Bo998/7-3 of the Schwerpunktprogramm 1167 by the Deutsche Forschungsgemeinschaft.

References

ARAKAWA, A., W.H. SCHUBERT, 1974: Interaction of a cumulus cloud ensemble with the large scale environment: Part I. – J. Atmos. Sci. **31**, 674–701.

BECHTOLD, P., E. BAZILE, F. GUICHARD, P. MASCARD, E. RICHARD, 2001: A mass flux convection scheme for regional and global models. – Quart. J. Roy. Meteor. Soc. **127**, 869–886.

BETTS, A.K., 1986: A new convective adjustment scheme. Part I: Observational and theoretical basis. – Quart. J. Roy. Meteor. Soc. **112**, 677–692.

BRYAN, G.H., J.C. WYNGAARD, J.M. FRITSCH, 2003: Resolution requirements for the simulation of deep moist convection. – Mon. Wea Rev. **131**, 2394–2416.

CHARNEY, J., A. ELIASSEN, 1964: On the growth of the hurricane depression. – J. Atmos. Sci. **21**, 75–81.

CHEN, S.-H., Y.-L. LIN, 2005: Effects of moist Froude number and CAPE on a conditionally unstable flow over a mesoscale mountain ridge. – J. Atmos. Sci. **62**, 331–350.

DOMS, G., U. SCHAETTLER, 2002: A description of the nonhydrostatic regional model LM. Part I: Dynamics and Numerics Consortium for small scale modelling. – Deutscher Wetterdienst, Offenbach, Germany (also available at www.cosmo-model.org).

FRITSCH, J.M., C.F. CHAPPELL, 1980: Numerical prediction of convectively driven mesoscale pressure systems. Part I: Convective parameterizations. – J. Atmos. Sci. **37**, 1722–1733.

GREGORY, D., P. R. ROWNTREE, 1990: A mass flux convection scheme with representation of cloud ensemble characteristics and stability dependent closure. – Mon. Weather Rev. **118**, 1483–1506.

GREGORY, D., R. KERSHAW, P.M. INNES, 1997: Parameterization of momentum transport by convection. II: Tests in single-column and general circulation models. – Quart. J. Roy. Meteor. Soc. **123**, 1153–1183.

KAIN, J.S., 2004: The Kain-Fritsch convective parameterization: An update. – J. Appl. Meteor. **43**, 170–181.

KAIN, J.S., J.M. FRITSCH, 1993: Convective parameterization for mesoscale models: The Kain-Fritsch scheme. – Meteor. Monographs **24**, 165–170.

KUANG, Z., C.S. BRETHERTON, 2006: A mass flux scheme view of a high resolution simulation of a transition from shallow to deep cumulus convection. – J. Atmos. Sci. **63**, 1895–1909.

KUELL, V., A. BOTT, 2008: A hybrid convection scheme for use in nonhydrostatic numerical weather prediction models. – Meteorol. Z. **17**, 775–783.

—, —, 2009: Application of the hybrid convection parameterization scheme hymacs to different meteorological situations. – Atmos. Res. **94**, 743–753.

KUELL, V., A. GASSMANN, A. BOTT, 2007: Towards a new hybrid cumulus parameterisation scheme for use in nonhydrostatic weather prediction models. – Quart. J. Roy. Meteor. Soc. **133**, 479–490.

KUO, H.L., 1965: On formation and intensification of tropical cyclones through latent heat release by cumulus convection. – J. Atmos. Sci. **22**, 40–63.

MANABE, S., R.F. STRICKLER, 1964: Thermal equilibrium of the atmosphere with a convective adjustment. – J. Atmos. Sci. **21**, 361–385.

MANABE, S., J. SMAGORINSKI, R.F. STRICKLER, 1965: Simulated climatology of a general circulation model with a hydrological cycle. – Mon. Wea Rev. **93**, 769–798.

MONCRIEFF, M.W., C. LIU, 2006: Representing convective organization in prediction models by a hybrid strategy. – J. Atmos. Sci. **63**, 3404–3420.

OGURA, Y., H.R. CHO, 1973: Diagnostic determination of cumulus populations from large scale variables. – J. Atmos. Sci. **30**, 1276–1286.

TIEDTKE, M., 1989: A comprehensive mass flux scheme for cumulus parameterization in large scale models. – Mon. Wea. Rev. **117**, 1779–1800.

WEISMAN, M.L., J.B. KLEMP, 1982: The dependence of numerically simulated convective storms on vertical wind shear and buoyancy. – Mon. Weather Rev. **110**, 504–520.

WEISMAN, M.L., R. ROTUNNO, 2004: 'a theory for strong long-lived squall lines' revisited. – J. Atmos. Sci. **61**, 361–382.